Controlling phase of arbitrary polarizations using both the geometric phase and the propagation phase

Lin Wu,[1,2,*] Jin Tao,[1,2,†] and Guoxing Zheng[3,1]

[1]*State Key Laboratory of Optical Communication Technologies and Networks, Wuhan Research Institute of Posts and Telecommunications, Wuhan, China*

[2]*National Information Optoelectronics Innovation Center, Wuhan Research Institute of Posts and Telecommunications, Wuhan, China*

[3]*School of Electronic Information, Wuhan University, Wuhan, China*

(Received 19 April 2018; published 28 June 2018)

Subwavelength spatial control of phase using metasurfaces is attractive for practical applications such as flat lens, vector beam generator, ultrathin wave-plate and high-resolution holography. All-dielectric metasurfaces provide two phase modulation mechanisms, which are propagation phase dependent on the dimension of meta-atoms and geometric phase dependent on the orientation of meta-atoms. Recently, it was proposed that by combining geometric phase and propagation phase, arbitrary and independent phase profiles can be imposed on a pair of orthogonal polarizations. However, a succinct expression of phase change introduced during an arbitrary polarization conversion process has not been presented. Here, we derive the geometric phase for the general case of nonorthogonal polarization conversions. Through the numerical simulations of a metasurface orbital angular momentum generator under both circular and elliptical polarization illuminations, we verify our theoretical analyses. This work presents the mechanism of controlling polarization and phase of arbitrary polarizations using both geometric phase and propagation phase, which exhibits the potential to enrich the capacity of polarization multiplexed metasurfaces.

DOI: 10.1103/PhysRevB.97.245426

I. INTRODUCTION

The rapidly evolving field of metasurfaces suggests a promising novel technology for controlling the characteristics of light using ultrathin optical components [1–5]. It is particularly interesting to engineer the wavefront of light using metasurface in either transmission or reflection mode, leading to applications such as beam steering [6], beam splitter [7], metalens [8,9], vector beam generator [10,11], and high-resolution holography [12,13]. Although these topics and functionalities have been considered through conventional diffractive optics or Fourier optics [14,15], and experimentally realized by using liquid-crystal-based optical modulators [16], metasurfaces show advantages due to their capability of subwavelength spatial control of light. It has been demonstrated that metasurfaces can optimize conventional optical components performances such as resolution and efficiency by emulating unwanted diffraction orders [17,18]. Moreover, metasurfaces can also achieve properties that are not available using conventional optical components. Here, we name a few examples. In the design of metalens, the achromatic metalens using just one layer of metasurface has been demonstrated recently [19–21]. This is enabled by engineering the dispersions of meta atoms to compensate the dispersionless geometric (or Pancharatnam-Berry) phase. In the design for generating a vector beam, metasurface can manipulate the polarization and phase profiles of the outcome light simultaneously [22]. In the research of holography, commercial liquid-crystal-based devices provide amplitude-only or phase-only modulation [16]. In contrast, metasurface enables simultaneous control of amplitude and phase, which paves the way to high-resolution optical holography [23,24]. Moreover, as meta-atoms respond differently to the polarization [7,25,26], wavelength [27–30], and illumination angle of incident light [31], various multiplexed metasurfaces have been proposed [32,33].

Generally, there are two phase modulation mechanisms of dielectric metasurfaces—propagation phase and geometric phase, which are employed for controlling the phase of linear and circular polarization, respectively. The linearly polarized wave passing through an array of nanobricks with large aspect ratios [7] is imposed by a propagation phase, which is dependent on the size of the nanobricks. As long as there is a large database of various meta-atoms, one can find an arbitrary combination of propagation phases for two orthogonal linear polarizations. As a result, independent phase control based on two orthogonal linear polarizations can be realized. For two orthogonal circular polarizations, the geometric phase is employed to impose phases on transmitted or reflected waves. The nature of the geometric phase keeps the two phase profiles equal and opposite [34], while it has been shown that the geometric phase can also give rise to independent phase control by using advanced holographic multiplexing algorithms [35]. Very recently, a strategy of combining both propagation phase and geometric phase is proposed to independently control the phase introduced during conversion between two orthogonal circular polarizations [36,37]. This method can be extended to work for any pair of orthogonal states of polarization. Currently, the applicability of metasurfaces is limited to the

*wulin@wri.com.cn

†taojin@wri.com.cn

transmissions of linear polarizations or the conversions of circular polarizations. Expanding the input and output polarizations of metasurfaces to arbitrary polarizations can boost the functionalities of metasurface as wavefront generators or sensors. For example, one metasurface can generate multiple different wavefronts by setting the polarizations of both incident and output waves [38]. However, the design strategy for elliptical polarization multiplexed metasurfaces is not clear yet, as it lacks of a succinct expression for the geometric phase under elliptical polarization illumination. Moreover, it would also be interesting to consider the phase changes introduced during conversions between two arbitrary but not necessary orthogonal polarizations, which is absent in current literature. By employing arbitrary combinations of input and output polarizations, one polarization multiplexed metasurface may carry multiple wavefronts.

In this paper, we present a comprehensive study on controlling the phase change introduced during conversions of light by using both geometric phase and propagation phase. Starting from the Jones calculus [39], we give an expression of geometric phase for conversions between two arbitrary polarizations. It is worth noting that the analysis method can work for conversion processes between pairs of both orthogonal and nonorthogonal polarizations. We also design a metasurface which responds independently to two orthogonal circular polarizations at telecommunication frequency. Furthermore, the incidence of an elliptically polarized wave is also considered. Rather than discussing the conversions between two orthogonal elliptical polarizations, we discuss the conversions between two counterrotating elliptical polarizations with the same ellipticity, and those between two corotating elliptical polarizations with different ellipticity. It is found that although both circular and elliptical polarizations can be manipulated using both propagation phase and geometric phase, it still needs additional amplitude modulation when constructing holograms using elliptical polarizations. This investigation provides an extension to the theory of geometric phase, which may serve as a guide to design novel polarization multiplexed metasurfaces for various applications in the near future.

II. THEORETICAL ANALYSES

A. Geometric phase introduced during conversions between orthogonal polarizations

The geometric phase of the transmitted wave with inversed circular polarization only depends on the orientation of meta-atoms. Here, we use the Jones matrix to analyze a more general case of conversions between two orthogonal elliptical polarizations. The meta-atoms used are rectangle silicon nanobricks with negligible linear polarization conversions under illumination along the z direction, as depicted in Fig. 2(a). The corresponding Jones matrix that connects the generally complex amplitudes of the incident and the transmitted linearly polarized waves is

$$\mathbf{T} = \begin{pmatrix} t_{xx}e^{i\phi_{xx}} & 0 \\ 0 & t_{yy}e^{i\phi_{yy}} \end{pmatrix}, \tag{1}$$

where t_{xx} and t_{yy} are the transmission coefficients for x- and y-polarized waves, respectively, and ϕ_{xx} and ϕ_{yy} are the propagation phases for x- and y-polarized waves, respectively. It has been widely known that the Jones matrix of a meta-atom with a rotating angle θ is

$$\mathbf{T}(\theta) = \begin{pmatrix} \cos\theta & \sin\theta \\ -\sin\theta & \cos\theta \end{pmatrix}^{-1} \mathbf{T} \begin{pmatrix} \cos\theta & \sin\theta \\ -\sin\theta & \cos\theta \end{pmatrix}. \tag{2}$$

To consider the transmission of elliptical polarizations, it is useful to have the Jones matrix in the arbitrary basis, as

$$\begin{aligned} \mathbf{T}(\chi,\delta) &= \begin{pmatrix} t_{++} & t_{+-} \\ t_{-+} & t_{--} \end{pmatrix} \\ &= \begin{pmatrix} \cos\chi & \sin\chi \\ e^{i\delta}\sin\chi & -e^{i\delta}\cos\chi \end{pmatrix}^{-1} \\ &\quad\times \mathbf{T} \begin{pmatrix} \cos\chi & \sin\chi \\ e^{i\delta}\sin\chi & -e^{i\delta}\cos\chi \end{pmatrix}, \end{aligned} \tag{3}$$

where $+$ and $-$ denote a pair of orthogonal polarization states of

$$\begin{pmatrix} \cos\chi \\ e^{i\delta}\sin\chi \end{pmatrix} \quad \text{and} \quad \begin{pmatrix} \sin\chi \\ -e^{i\delta}\cos\chi \end{pmatrix},$$

respectively. Here, δ and χ define arbitrary polarization states, and $\tan\chi$ represents the ellipticity of polarization. By inserting the Jones matrix in Eq. (2) into Eq. (3), we can obtain the transmission and conversion of arbitrary polarization passing through a meta-atom with a rotational angle θ. As a result, the two conversions are

$$\begin{aligned} t_{+-}(\chi,\delta,\theta) = {}& \tfrac{1}{2}(t_{xx}e^{i\phi_{xx}} - t_{yy}e^{i\phi_{yy}})[\sin 2\chi\ \cos 2\theta \\ & + (e^{-i\delta}\sin^2\chi - e^{i\delta}\cos^2\chi)\sin 2\theta], \end{aligned} \tag{4}$$

$$\begin{aligned} t_{-+}(\chi,\delta,\theta) = {}& \tfrac{1}{2}(t_{xx}e^{i\phi_{xx}} - t_{yy}e^{i\phi_{yy}})[\sin 2\chi\ \cos 2\theta \\ & - (e^{-i\delta}\cos^2\chi - e^{i\delta}\sin^2\chi)\sin 2\theta]. \end{aligned} \tag{5}$$

In Eqs. (4) and (5), the propagation phases ϕ_{xx} and ϕ_{yy} are the phase delay of the waveguide modes existing in the tall nanobricks. Hence, they can be tailored by employing different sized nanobricks with various effective propagation constants. The angles of $[\sin 2\chi\ \cos 2\theta - (e^{\pm i\delta}\cos^2\chi - e^{\mp i\delta}\sin^2\chi)\sin 2\theta]$ are the phase changes due to the rotational angle θ of nanobricks, which can be regarded as the generalized geometric phases. Other than the rotational angles, these phase changes are also determined by the input and output polarizations. We plot these phase changes for different polarizations in Fig. 1. For the circular polarization ($\delta = 90^\circ$, $\chi = 45^\circ$) incidences, the geometric phase is 2θ, corresponding to the Pancharatnam-Berry phase. And the amplitude changes have a constant value of 1. For the elliptical polarization incidences, the geometric phase still covers a

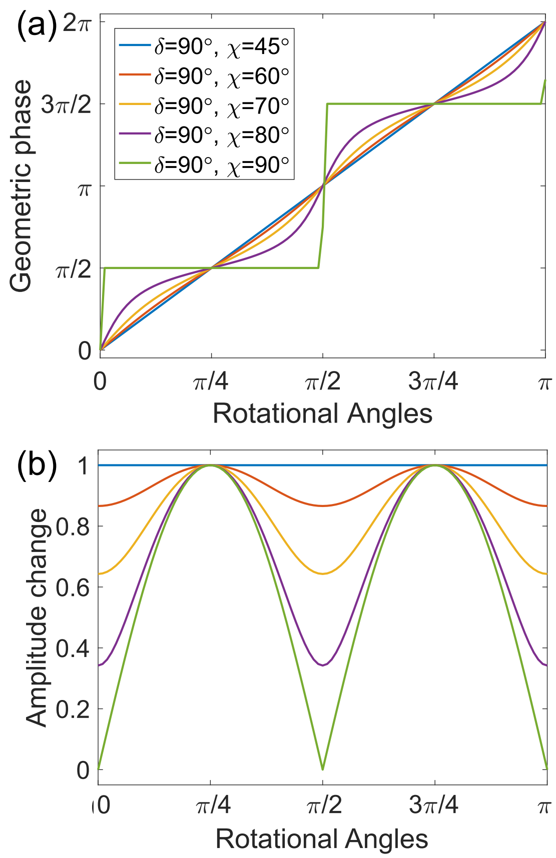

FIG. 1. The dependence of (a) geometric phase and (b) amplitude change introduced during conversions between two orthogonal polarizations on the rotational angle of a meta-atom.

range from 0 to 2π when the meta-atom rotates from 0 to π, but the relationship between the geometric phase and θ is no longer linear. More importantly, the amplitude changes exhibit different values for different rotational angles, which will reduce the performance of holography using elliptically polarized light. Finally, when it comes to the linear polarizations ($\delta = 90^\circ$, $\chi = 90^\circ$), the geometric phases vanish.

B. Geometric phase introduced during conversions between nonorthogonal polarizations

The aforementioned analysis method is not only applicable to the orthogonal basis, as the Jones matrix can be changed into an arbitrary not necessarily orthogonal base. To obtain the amplitude and phase changes during arbitrary polarization conversions, one could first implement the rotation matrix operation in the linear polarization base [Eq. (2)], and then transfer the Jones matrix into the specified base. Here, we discuss two cases: the conversions between two counterrotating polarizations with the same ellipticity and the conversions between two corotating polarizations with different ellipticity. For the first case, the Jones matrix can be expressed as

$$\mathbf{T}'(\chi,\delta) = \begin{pmatrix} t'_{++} & t'_{+-} \\ t'_{-+} & t'_{--} \end{pmatrix} = \begin{pmatrix} \cos\chi & \cos\chi \\ e^{i\delta}\sin\chi & -e^{i\delta}\sin\chi \end{pmatrix}^{-1} \times \mathbf{T}\begin{pmatrix} \cos\chi & \cos\chi \\ e^{i\delta}\sin\chi & -e^{i\delta}\sin\chi \end{pmatrix}. \tag{6}$$

The two elements for conversions in Eq. (6) are as follows:

$$t'_{+-}(\chi,\delta,\theta) = \frac{1}{2}(t_{xx}e^{i\phi_{xx}} - t_{yy}e^{i\phi_{yy}})\frac{\sin 2\chi\ \cos 2\theta + (e^{-i\delta}\cos^2\chi - e^{i\delta}\sin^2\chi)\sin 2\theta}{\sin 2\chi}, \tag{7}$$

$$t'_{-+}(\chi,\delta,\theta) = \frac{1}{2}(t_{xx}e^{i\phi_{xx}} - t_{yy}e^{i\phi_{yy}})\frac{\sin 2\chi\ \cos 2\theta - (e^{-i\delta}\cos^2\chi - e^{i\delta}\sin^2\chi)\sin 2\theta}{\sin 2\chi}. \tag{8}$$

It is notable that when $\chi = 45^\circ$, Eqs. (7) and (8) become identical to Eqs. (4) and (5). For the second case, the Jones matrix is

$$\mathbf{T}''(\chi,\delta) = \begin{pmatrix} t''_{++} & t''_{+-} \\ t''_{-+} & t''_{--} \end{pmatrix} = \begin{pmatrix} \cos\chi_1 & \cos\chi_2 \\ e^{i\delta}\sin\chi_1 & e^{i\delta}\sin\chi_2 \end{pmatrix}^{-1}\mathbf{T}\begin{pmatrix} \cos\chi_1 & \cos\chi_2 \\ e^{i\delta}\sin\chi_1 & e^{i\delta}\sin\chi_2 \end{pmatrix}. \tag{9}$$

Here, the symbols + and − denote the polarizations with ellipticity of $\tan\chi_1$ and $\tan\chi_2$, respectively. One of the conversions between them can be calculated as

$$t''_{-+}(\chi_1,\chi_2,\delta,\theta) = \frac{1}{2}(t_{xx}e^{i\phi_{xx}} - t_{yy}e^{i\phi_{yy}})\frac{-\sin 2\chi_1\cos 2\theta + (e^{-i\delta}\cos^2\chi_1 - e^{i\delta}\sin^2\chi_1)\sin 2\theta}{\sin\chi_2 - \chi_1}. \tag{10}$$

From Eq. (10), the geometric phase is only dependent on the incident polarizations, while the amplitude change is determined by both incident and output polarizations.

In Table I, we summarize the geometric phases and amplitude changes in the aforementioned three cases described by Eqs. (3), (6), and (9). We show both elliptical polarizations ($\delta = 90^\circ$, $\chi \neq 45^\circ$) and the general polarizations with $\delta \neq 90^\circ$, $\chi \neq 45^\circ$ for all three cases. The first row denotes the well-known case of the Pancharatnam-Berry phase for circular polarizations. The second row denotes the conversion processes of a pair of orthogonal polarizations, while rows 3 and 4 denote those of a pair of nonorthogonal polarizations. The three processes introduce the same geometric phase but different amplitude changes. The rows 5–7 in Table I denote the more general cases where both δ and χ can be arbitrary values. It is worth noting that the geometric phases for the two

TABLE I. Summary of geometric phase and amplitude change introduced during conversions between arbitrary polarization states.

Input polarization	Output polarization	Geometric phase	Amplitude change
$\binom{1}{\mp i}$	$\binom{1}{\pm i}$	$\mp 2\theta$	1
$\binom{\cos\chi}{\mp i\sin\chi}$	$\binom{\sin\chi}{\pm i\cos\chi}$	$\mp\arctan\frac{\tan 2\theta}{\sin 2\chi}$	$\sqrt{(\sin 2\chi\cos 2\theta)^2+\sin^2 2\theta}$
$\binom{\cos\chi}{\mp i\sin\chi}$	$\binom{\cos\chi}{\pm i\sin\chi}$	$\mp\arctan\frac{\tan 2\theta}{\sin 2\chi}$	$\frac{\sqrt{(\sin 2\chi\cos 2\theta)^2+\sin^2 2\theta}}{\lvert\sin 2\chi\rvert}$
$\binom{\cos\chi_1}{i\sin\chi_1}$	$\binom{\cos\chi_2}{i\sin\chi_2}$	$\arctan\frac{\tan 2\theta}{\sin 2\chi_1}$	$\frac{\sqrt{(\sin 2\chi_1\cos 2\theta)^2+\sin^2 2\theta}}{\lvert\sin\chi_2-\chi_1\rvert}$
$\binom{\cos\chi}{e^{\mp i\delta}\sin\chi}$	$\binom{\sin\chi}{e^{\pm i\delta}\cos\chi}$	$\mp\arctan\frac{a}{b-c}$	$\sqrt{a^2+(b-c)^2}$
$\binom{\cos\chi}{e^{\mp i\delta}\sin\chi}$	$\binom{\cos\chi}{e^{\pm i\delta}\sin\chi}$	$\mp\arctan\frac{a}{b\pm c}$	$\frac{\sqrt{a^2+(b\pm c)^2}}{\lvert\sin 2\chi\rvert}$
$\binom{\cos\chi_1}{e^{i\delta}\sin\chi_1}$	$\binom{\cos\chi_2}{e^{i\delta}\sin\chi_2}$	$\arctan\frac{a}{b-c}$	$\frac{\sqrt{a^2+(b-c)^2}}{\lvert\sin\chi_2-\chi_1\rvert}$

[a]$\sin\delta\sin 2\theta$.
[b]$\sin 2\chi\cos 2\theta$.
[c]$\cos\delta\cos 2\chi\sin 2\theta$.

conversion processes between two orthogonal polarizations have opposite values, while the geometric phases for the two conversions between two counterrotating polarizations with the same ellipticity can exhibit different absolute values.

III. DESIGNS AND RESULTS

In this section, we show examples for phase control during the conversion processes between two circular polarizations, two counterrotating elliptical polarizations with the same ellipticity, and two corotating elliptical polarizations with different ellipticity.

A. Polarization conversion involving change of δ

For converting δ of polarizations, one needs meta-atoms with $t_{xx}=t_{yy}$ and $\phi_{xx}=\phi_{yy}+\pi$ to achieve high conversions. By designing meta-atoms with various ϕ_{xx}, one can manipulate the phase of converted polarizations by using both geometric phase and propagation phase. The total phase changes from polarization state $-$ to $+$ and reversed process are

$$\psi_{+-}=\phi_{xx}-\varphi,\quad \psi_{-+}=\phi_{xx}+\varphi. \tag{11}$$

In Eq. (11), ϕ_{xx} is the propagation phase and φ is the geometric phase. Hence, the two total phase changes can be a set of arbitrary independent values. The geometric phase can be determined by appropriately choosing the rotational angle, while in order to obtain arbitrary value for the propagation phase, we simulated a number of silicon nanobricks with various dimensions functioning at the wavelength of 1550 nm. The results are summarized in Fig. 2. In the simulations, the refractive indexes of silica substrate and silicon nanobricks are taken as 1.46 and 3.45, respectively. The electric conductivity of silicon is 2.5×10^{-4} S/m. The periodic boundary condition is employed in the x and y directions. Figure 2(a) depicts the schematic diagram of one unit cell of the simulated meta-atom with a fixed height of $h=865$ nm and a lattice constant of $p=750$ nm. Within the boxes in Fig. 2, we can find meta-atoms with identical $\phi_{xx}-\phi_{yy}$ of π, but different ϕ_{xx} ranging from 0 to 2π. Moreover, the transmissions for linear polarizations are relatively high, as shown in Figs. 2(c) and 2(d). Here, we choose a set of 12 meta-atoms with the total phase changes ranging from 0 to 2π and 0 to 4π for t_{+-} and t_{-+}, respectively. Then, the required propagation phases and geometric phases can be calculated by Eq. (11). The dimensions of each meta-atom and corresponding propagation phase and geometric phase are shown in Table II. The rotational angle of each meta-atom is calculated using the expressions in Table I. Using these 12 meta-atoms, we design a metasurface orbital angular momentum (OAM) generator, exhibiting independent phase manipulation over a pair of circular polarizations and two counterrotating elliptical polarizations with the same ellipticity.

We perform the simulations for the illuminations under left-handed and right-handed circularly polarized (LCP and RCP) Gaussian beams of the wavelength of 1550 nm. The designed 12 nanobricks in Table II are arranged in a circular manner. So the phase profiles along the azimuthal angles ranging from 0 to 2π and 0 to 4π for conversion from RCP to LCP waves and that from LCP to RCP waves, respectively. The corresponding topological charges of OAM beams are 1 and 2. For simplifying the simulations, we only simulate a metasurface consisting of 20×20 meta-atoms. The phase and normalized amplitude distributions at the surface with a distance of 5500 nm away from the substrate plane of the metasurface are plotted in Fig. 3. From Fig. 3(a), the vector RCP beam from LCP incidence has a topological charge of 2. In conventional metasurfaces, the topological charge of the vector LCP beam from RCP incidence should be -2, while in this design, this parameter turns out to be 1, as shown in Fig. 3(c). The amplitude distributions in Figs. 3(b) and 3(d) show good doughnut shapes.

In our designed metasurface, the meta-atoms show the same amplitude change while different phase changes to x- and y-polarization incidences, which means that the proposed metasurface can only implement conversions between two counterrotating elliptical polarizations with the same ellipticity. Figure 4 depicts the calculated results for incidences of elliptically polarized Gaussian beams. From the previous analysis, the introduced geometric phases still vary from 0 to 2π when the meta-atoms rotate by an angle from 0 to π. The differences from the case of circular polarization incidences are as follows: (1) the relationship between the geometric phase

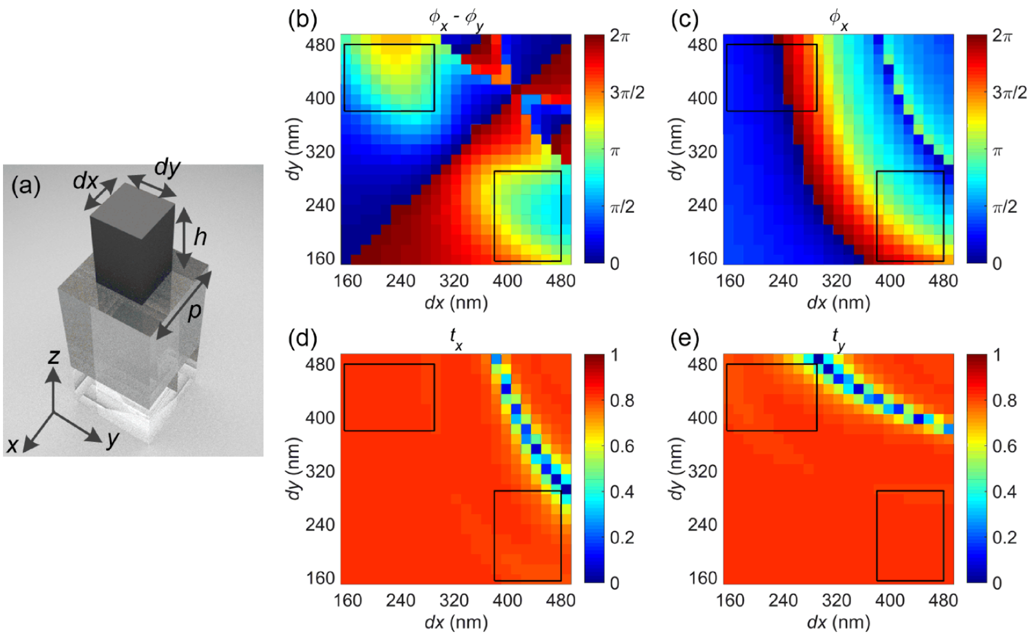

FIG. 2. Numerical results of transmissions of linear polarizations for meta-atoms with various dimensions. (a) Schematic of a unit cell of the proposed meta-atom. (b) The phase difference between transmission coefficients of x and y polarizations. (c) The phase of transmission coefficients of x polarization. (d) The amplitude of transmission coefficients of x polarization. (e) The amplitude of transmission coefficients of y polarization.

and the rotational angle of meta-atom is no longer linear; (2) the amplitude of conversion changes dramatically with respect to the rotation of meta-atoms. This coincides with the results in Fig. 4, where the phase singularities are still presented while the amplitude distributions do not display a perfect doughnut shape. Hence, to realize the OAM generator or even holography using elliptical polarization, it is necessary to modulate both phase and amplitude profiles using the results in Table I. To eliminate the amplitude variations during the conversions of elliptical polarizations, one can use the two maximum conversion coefficients at two rotational angles as shown in Fig. 1. However, this binary modulated beam shaping method produces desired intensity distributions only in the far field and carries energy in the unwanted higher-order modes [40].

TABLE II. Summary of meta-atoms with different propagation phases and geometric phases for a wavelength of 1550 nm.

ψ_{-+} (deg)	ψ_{+-} (deg)	ϕ_{xx} (deg)[a]	φ (deg)	dx (nm)	dy (nm)
0	0	0	0	235	397
60	30	45	15	165	470
120	60	90	30	450	275
180	90	135	45	415	261
240	120	180	60	397	235
300	150	225	75	470	165
0	180	90	−90	450	275
60	210	135	−75	415	261
120	240	180	−60	397	235
180	270	225	−45	470	165
240	300	270	−30	275	450
300	330	315	−15	261	415

[a] $\phi_{yy} = \phi_{xx} - 180^\circ$.

B. Polarization conversion involving change of χ

In this section, we consider the phase manipulation for conversions between two corotating elliptical polarizations with different ellipticity. To achieve high conversion, the meta-atoms should satisfy the following relationships for the transmission coefficients of linear polarizations:

$$\cos\chi_1 t_{xx} = \cos\chi_2, \quad \sin\chi_1 t_{yy} = \sin\chi_2, \quad \phi_{xx} = \phi_{yy}. \quad (12)$$

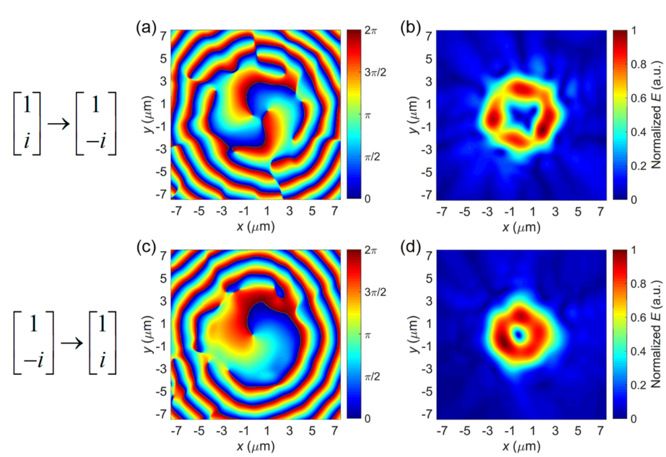

FIG. 3. The numerical results of the designed metasurfaces generating different OAM beams for different circular polarizations. (a) and (b) The phase and amplitude maps for conversions from LCP to RCP waves. (c) and (d) The phase and amplitude maps for conversions from RCP to LCP waves.

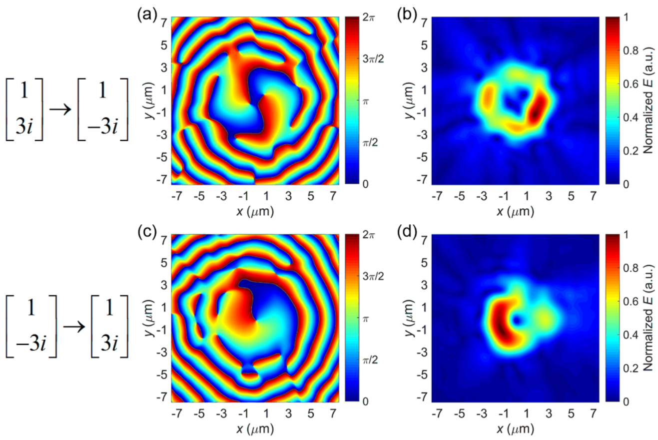

FIG. 4. The numerical results of the designed metasurfaces generating different phase profiles for different elliptical polarizations. (a) and (b) The phase and amplitude maps for conversions from left-handed to right-handed elliptical polarizations. (c) and (d) The phase and amplitude maps for conversions from right-handed to left-handed elliptical polarizations.

By inserting Eq. (12) into Eq. (10), we obtain

$$t''_{-+} = e^{i\phi_{xx}} \times \frac{\sin 2\chi_1 \cos 2\theta - \cos\delta\ \cos 2\chi_1 \sin 2\theta + i\ \sin\delta\ \sin 2\theta}{\sin 2\chi_1}. \tag{13}$$

The geometric phase and amplitude change can be fully determined by the polarization of incident wave. For example, the circular polarization incidence ($\delta = 90^\circ$, $\chi = 45^\circ$) can be converted to polarization with $\delta = 90^\circ$, $\chi = \chi_2$ imposed by the phase of $\phi_{xx} + 2\theta$. Recently, a lot of novel meta-atoms other than nanobrick or nanodisk have been proposed to exhibit different properties for x and y polarizations, such as C-shaped meta-atoms [31,41]. Unfortunately, we cannot use the geometric phase to control the phase of output beams here. Because $t_{xx} \neq t_{yy}$ means the meta-atoms are polarization sensitive, and rotation of meta-atoms will change the responses of metasurface to x- and y-polarized waves. Alternatively, one can find various meta-atoms to obtain a constant value for t_{xx}/t_{yy} and different values ranging from 0 to 2π for $\phi_{xx} = \phi_{yy}$, so as to control polarization and wavefront at the same time.

IV. CONCLUSION

In conclusion, we derived the geometric phases introduced during conversions between two circular polarizations, two counterrotating elliptical polarizations with the same ellipticity, and two corotating elliptical polarizations with different ellipticity. The expressions for phase and amplitude changes with respect to rotational angles of meta-atoms are summarized as references for the near future designs of novel polarization multiplexed metasurfaces. Moreover, geometric phase can cooperate with propagation phase to impose arbitrary and independent phase profiles on two different polarizations. The design strategy of controlling both polarization and wavefront of output beams is made clear through our analyses. However, different from the conversion between two orthogonal circular polarizations, the magnitude of conversion between two nonorthogonal polarizations changes dramatically with respect to the rotational angles, which may be addressed by simultaneous modulations of both phase and amplitude profiles. This work demonstrates the unique property of a metasurface to control the polarization and the phase profiles of arbitrary incident waves simultaneously, which may increase the capacity of optical communication systems by multiplexing various polarizations and OAM states. The further opportunities in simultaneously controlling both phase and polarization may be found in complex nanostructures [38] or two-dimensional materials [42,43].

ACKNOWLEDGMENTS

We wish to acknowledge the support of Wuhan Morning Light Plan of Youth Science and Technology (2017050304010324), National Natural Science Foundation of China (Grants No. 11574240 and No. 11774273), the Outstanding Youth Funds of Hubei Province (2016CFA034), and the Open Foundation of State Key Laboratory of Optical Communication Technologies and Networks, Wuhan Research Institute of Posts and Telecommunications (Grant No. OCTN-201605).

[1] H.-H. Hsiao, C. H. Chu, and D. P. Tsai, Small Methods **1**, 1600064 (2017).

[2] L. Zhang, S. Mei, K. Huang, and C. W. Qiu, Adv. Opt. Mater. **4**, 818 (2016).

[3] P. Genevet, F. Capasso, F. Aieta, M. Khorasaninejad, and R. Devlin, Optica **4**, 139 (2017).

[4] H.-T. Chen, A. J. Taylor, and N. Yu, Rep. Prog. Phys. **79**, 076401 (2016).

[5] N. Yu, P. Genevet, M. A. Kats, F. Aieta, J.-P. Tetienne, F. Capasso, and Z. Gaburro, Science **334**, 333 (2011).

[6] N. L. Tsitsas and C. A. Valagiannopoulos, J. Opt. Soc. Am. B **34**, D1 (2017).

[7] A. Arbabi, Y. Horie, M. Bagheri, and A. Faraon, Nat. Nanotechnol. **10**, 937 (2015).

[8] M. Khorasaninejad and F. Capasso, Science **358**, eaam8100 (2017).

[9] G. Zheng, W. Wu, Z. Li, S. Zhang, M. Q. Mehmood, P. He, and S. Li, Opt. Lett. **42**, 1261 (2017).

[10] Y. Yang, W. Wang, P. Moitra, I. I. Kravchenko, D. P. Briggs, and J. Valentine, Nano Lett. **14**, 1394 (2014).

[11] M. I. Shalaev, J. Sun, A. Tsukernik, A. Pandey, K. Nikolskiy, and N. M. Litchinitser, Nano Lett. **15**, 6261 (2015).

[12] G. Zheng, H. Mühlenbernd, M. Kenney, G. Li, T. Zentgraf, and S. Zhang, Nat. Nanotechnol. **10**, 308 (2015).

[13] Z.-L. Deng and G. Li, Mater. Today Phys. **3**, 16 (2017).

[14] S. V. Serak, D. E. Roberts, J.-Y. Hwang, S. R. Nersisyan, N. V. Tabiryan, T. J. Bunning, D. M. Steeves, and B. R. Kimball, J. Opt. Soc. Am. B **34**, B56 (2017).

[15] N. Mohammad, M. Meem, X. Wan, and R. Menon, Sci. Rep. **7**, 5789 (2017).
[16] Z. Zhang, Z. You, and D. Chu, Light: Sci. Appl. **3**, e213 (2014).
[17] L. Wang, S. Kruk, H. Tang, T. Li, I. Kravchenko, D. N. Neshev, and Y. S. Kivshar, Optica **3**, 1504 (2016).
[18] Z. Li, I. Kim, L. Zhang, M. Q. Mehmood, M. S. Anwar, M. Saleem, D. Lee, K. T. Nam, S. Zhang, B. Lukyanchuk, Y. Wang, G. Zheng, J. Rho, and C.-W. Qiu, ACS Nano **11**, 9382 (2017).
[19] S. Wang, P. C. Wu, V.-C. Su, Y.-C. Lai, C. Hung Chu, J.-W. Chen, S.-H. Lu, J.-W. Chen, B. Xu, C.-H. Kuan, T. Li, S. Zhu, and D. P. Tsai, Nat. Commun. **8**, 187 (2017).
[20] W. T. Chen, A. Y. Zhu, V. Sanjeev, M. Khorasaninejad, Z. Shi, E. Lee, and F. Capasso, Nat. Nanotechnol. **13**, 220 (2018).
[21] S. Wang, P. C. Wu, V.-C. Su, Y.-C. Lai, M.-K. Chen, H. Y. Kuo, B. H. Chen, Y. H. Chen, T.-T. Huang, J.-H. Wang, R.-M. Lin, C.-H. Kuan, T. Li, Z. Wang, S. Zhu, and D. P. Tsai, Nat. Nanotechnol. **13**, 227 (2018).
[22] Q. Guo, C. Schlickriede, D. Wang, H. Liu, Y. Xiang, T. Zentgraf, and S. Zhang, Opt. Express **25**, 14300 (2017).
[23] G.-Y. Lee, G. Yoon, S.-Y. Lee, H. Yun, J. Cho, K. Lee, H. Kim, J. Rho, and B. Lee, Nanoscale **10**, 4237 (2018).
[24] Z. Li, H. Cheng, Z. Liu, S. Chen, and J. Tian, Adv. Opt. Mater. **4**, 1230 (2016).
[25] C. Williams, Y. Montelongo, and T. D. Wilkinson, Adv. Opt. Mater. **5**, 1700811 (2017).
[26] Q. Wang, X. Zhang, E. Plum, Q. Xu, M. Wei, Y. Xu, H. Zhang, Y. Liao, J. Gu, J. Han, and W. Zhang, Adv. Opt. Mater. **5**, 1700277 (2017).
[27] W. Wan, J. Gao, and X. Yang, ACS Nano **10**, 10671 (2016).
[28] B. Wang, F. Dong, Q.-T. Li, D. Yang, C. Sun, J. Chen, Z. Song, L. Xu, W. Chu, Y.-F. Xiao, Q. Gong, and Y. Li, Nano Lett. **16**, 5235 (2016).
[29] X. Li, L. Chen, Y. Li, X. Zhang, M. Pu, Z. Zhao, X. Ma, Y. Wang, M. Hong, and X. Luo, Sci. Adv. **2**, e1601102 (2016).
[30] W. Zhao, B. Liu, H. Jiang, J. Song, Y. Pei, and Y. Jiang, Opt. Lett. **41**, 147 (2016).
[31] S. M. Kamali, E. Arbabi, A. Arbabi, Y. Horie, M. S. Faraji-Dana, and A. Faraon, Phys. Rev. X **7**, 041056 (2017).
[32] K. Huang, Z. Dong, S. Mei, L. Zhang, Y. Liu, H. Liu, H. Zhu, J. Teng, B. Luk'yanchuk, J. K. Yang, and C.-W. Qiu, Laser Photonics Rev. **10**, 500 (2016).
[33] F. Liu, A. Pitilakis, M. S. Mirmoosa, O. Tsilipakos, X. Wang, A. C. Tasolamprou, S. Abadal, A. Cabellos-Aparicio, E. Alarcón, C. Liaskos, N. V. Kantartzis, M. Kafesaki, E. N. Economou, C. M. Soukoulis, and S. Tretyakov, arXiv:1803.04252.
[34] D. Wen, F. Yue, G. Li, G. Zheng, K. Chan, S. Chen, M. Chen, K. F. Li, P. W. H. Wong, K. W. Cheah, E. Yue Bun Pun, S. Zhang, and X. Chen, Nat. Commun. **6**, 8241 (2015).
[35] Q. Wei, L. Huang, X. Li, J. Liu, and Y. Wang, Adv. Opt. Mater. **5**, 1700434 (2017).
[36] J. P. Balthasar Mueller, N. A. Rubin, R. C. Devlin, B. Groever, and F. Capasso, Phys. Rev. Lett. **118**, 113901 (2017).
[37] R. C. Devlin, A. Ambrosio, N. A. Rubin, J. P. B. Mueller, and F. Capasso, Science **358**, 896 (2017).
[38] Z.-L. Deng, J. Deng, X. Zhuang, S. Wang, K. Li, Y. Wang, Y. Chi, X. Ye, J. Xu, G. P. Wang, R. Zhao, X. Wang, Y. Cao, X. Cheng, G. Li, and X. Li, Nano Lett. **18**, 2885 (2018).
[39] C. Menzel, C. Rockstuhl, and F. Lederer, Phys. Rev. A **82**, 053811 (2010).
[40] S. Keren-Zur, O. Avayu, L. Michaeli, and T. Ellenbogen, ACS Photonics **3**, 117 (2016).
[41] A. Forouzmand and H. Mosallaei, Adv. Opt. Mater. **5**, 1700147 (2017).
[42] I. Crassee, J. Levallois, A. L. Walter, M. Ostler, A. Bostwick, E. Rotenberg, T. Seyller, D. van der Marel, and A. B. Kuzmenko, Nat. Phys. **7**, 48 (2011).
[43] C. A. Valagiannopoulos, M. Mattheakis, S. N. Shirodkar, and E. Kaxiras, J. Phys. Commun. **1**, 045003 (2017).